Aku Riihelä, Vesa Laine, Terhikki Manninen, Timo Palo, and Timo Vihma. 2010. Validation of the Climate-SAF surface broadband albedo product: Comparisons with in situ observations over Greenland and the ice-covered Arctic Ocean. Remote Sensing of Environment, volume 114, number 11, pages 2779-2790. doi:10.1016/j.rse.2010.06.014. © 2010 Elsevier. Reprinted with permission from Elsevier.
Remote Sensing of Environment 114 (2010) 2779–2790

Contents lists available at ScienceDirect

Remote Sensing of Environment

journal homepage: www.elsevier.com/locate/rse

Validation of the Climate-SAF surface broadband albedo product: Comparisons with in situ observations over Greenland and the ice-covered Arctic Ocean

Aku Riihelä [a,*], Vesa Laine [a], Terhikki Manninen [a], Timo Palo [b], Timo Vihma [a]

[a] Finnish Meteorological Institute, P.O. Box 503, FI-00101 Helsinki, Finland
[b] Department of Geography, University of Tartu, Vanemuise 46, 51014 Tartu, Estonia

ARTICLE INFO

Article history:
Received 15 March 2010
Received in revised form 22 June 2010
Accepted 23 June 2010

Keywords:
Albedo
Snow
Sea ice
Validation
AVHRR

ABSTRACT

This paper describes a validation study performed by comparing the Climate-SAF Surface Albedo Product (SAL) to ground truth observations over Greenland and the ice-covered Arctic Ocean. We compare Advanced Very High Resolution Radiometer (AVHRR)-based albedo retrievals to data from the Greenland Climate Network (GCN) weather stations and the floating ice station Tara for polar summer 2007. The AVHRR dataset consists of 2755 overpasses. The overpasses are matched to in situ observations spatially and temporally. The SAL algorithm presented here derives the surface broadband albedo from AVHRR channels 1 and 2 using an atmospheric correction, temporal sampling of an empirical Bidirectional Reflectance Distribution Function (BRDF), and a narrow-to-broadband conversion algorithm. The satellite product contains algorithms for snow, sea ice, vegetation, bare soil, and water albedo. At the Summit and DYE-2 stations on the Greenland ice sheet, instantaneous SAL RMSE is 0.073. The heterogeneous surface conditions at satellite pixel scale over the stations near the Greenland west coast increase RMSE to >0.12. Over Tara, the instantaneous SAL RMSE is 0.069. The BRDF sampling approach reduces RMSE over the ice sheet to 0.053, and to 0.045 over Tara. Taking into account various sources of uncertainty for both satellite retrievals and in situ observations, we conclude that SAL agrees with in situ observations within their limits of accuracy and spatial representativeness.

1. Background

Surface albedo, defined as the ratio of reflected to incoming radiation fluxes, is acknowledged to be one of the dominating factors of the Earth's radiation budget (Dickinson, 1983). Snow and ice have the highest albedo of all surface types on the Earth. Variations in the surface albedo of the Arctic region have a large effect on the radiation budget of the earth–atmosphere system and thereby on the global climate (Xiong et al., 2002). Over the recent years, scientific and political concern over climate change has focused increased attention to the Earth's climate system. The Polar regions are of particular interest because studies indicate that they are the most vulnerable to climate change, and will therefore be the first to exhibit effects related to climate change (Holland & Bitz, 2003; Manabe & Stouffer, 1980; Moritz et al., 2002; Perovich et al., 2002; Serreze et al., 2009). Variations in the surface albedo play a key role in the process through the well-known snow and ice albedo feedback effect (Curry et al., 1996; Manabe & Stouffer, 1980; Perovich et al., 2007). The studies also agree that surface albedo and its variability in Polar regions is one of the least well-known factors in climate models. This uncertainty causes variance in the model results and makes it more difficult to predict the future climate.

To improve the modeling accuracy, more high-quality observations of the surface albedo of the Polar regions are needed. In situ monitoring is impractical over large, remote and sparsely populated areas. Therefore satellite observations are the most useful way forward. To respond to this growing need for continuous observations of the Arctic surface albedo, we are implementing a novel surface broadband albedo product. The product covers the area from the North Pole to 67.4° North latitude, although the rectangular product area extends down to 57.8° North latitude in the corners (see Fig. 1(b)). The product is based on the Advanced Very High Resolution Radiometer (AVHRR) instruments on board NOAA-17, -18 and MetOp satellites. The product area covers the entire Arctic ice cap, as well as the entirety of Greenland. The goal of this study is to discuss the new Arctic Surface Albedo Product (SAL), describe its validation over Arctic reference sites and draw conclusions about its accuracy based on the results.

Previously surface albedo observations of the Arctic from polar-orbiting satellites have been studied by several authors, for example by Knap and Oerlemans (1996) and Stroeve et al. (1997) for operational AVHRR, by Key et al. (2001), Stroeve (2001), Stroeve et al. (2001) and Laine (2004) for AVHRR polar pathfinder dataset, by DeAbreu et al. (1994), Lindsay and Rothrock (1994), Comiso (2001) and Xiong et al. (2002) for Arctic sea ice with AVHRR, and by Liang et al. (2005) and Stroeve et al. (2006) for Moderate Resolution Imaging Spectroradiometer (MODIS). The new Arctic SAL product seeks to provide comprehensive weekly and monthly surface broadband albedo

* Corresponding author. Tel.: +358 9 1929 4152; fax: +358 9 1929 4603.
E-mail address: aku.riihela@fmi.fi (A. Riihelä).

0034-4257/$ – see front matter © 2010 Elsevier Inc. All rights reserved.
doi:10.1016/j.rse.2010.06.014

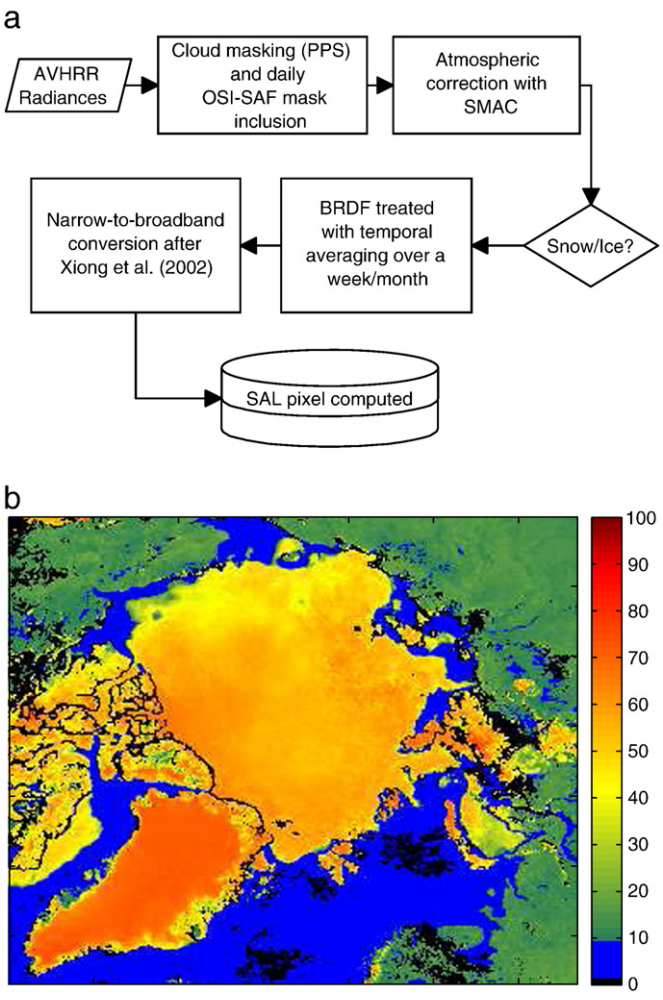

Fig. 1. Operational SAL snow albedo generation process and an example of the produced temporal means products.

products including dedicated algorithms for snow and sea ice albedo retrievals. A novel feature in SAL is the determination of sea ice extent using a microwave observation-based sea ice product from the Ocean and Sea Ice Satellite Application Facility (OSI-SAF) (Breivik et al., 2001). This reduces misclassifications between clouds and sea ice and improves product quality and stability over the Polar Ice Cap. The features of the Arctic SAL product shall be described fully in the next section.

This paper is organized as follows: We shall first introduce the satellite albedo validation dataset and the general process of deriving an instantaneous SAL product from a NOAA/MetOp overpass. Then, we shall describe the reference datasets used to assess the product quality. These datasets are from the Greenland Climate Network (GC-Net) and the Tara schooner expedition observations. We shall then show the validation results and finally discuss issues related to our study methodology and draw conclusions from the study.

2. Data and methodology

2.1. The SAL product generation

The Arctic SAL product from AVHRR describes the surface broadband albedo at the waveband of 0.25–2.5 μm. The operational product is computed from the NOAA-17, -18 and MetOp satellites, using AVHRR channels 1 and 2. Retrieval of the surface albedo is performed at nominal AVHRR spatial resolution (1.09 km at nadir). User-distributed weekly and monthly mean products are resampled into 15×15 km spatial resolution. The algorithm is currently being updated according to results and recommendations from this study. References to the SAL algorithm will henceforth be for the new algorithm shown below. The SAL algorithm employed prior to 2010 used the Manalo-Smith algorithm (Manalo-Smith et al., 1998) to account for snow Bidirectional Reflectance Distribution Function (BRDF) on the instantaneous level. This approach has now been superseded by the approach described in this paper. The effects of algorithm changes and limitations are discussed in Section 4.

The retrieval of AVHRR SAL is described in Fig. 1(a). Fig. 1(b) shows the extent of SAL coverage and an example of the final weekly product from 2009. In the following we shall discuss some of the most important considerations for each SAL processing stage.

2.1.1. Calibration and cloud mask generation

Observed radiances are calibrated into Top of Atmosphere (TOA) reflectances in the preprocessing performed by the Polar Platform System (PPS) (Dybbroe et al., 2005). A cloud mask is generated at this stage to delineate cloud-contaminated pixels. The cloud masking algorithm is based on a multi-spectral thresholding technique, applied to each pixel of the satellite overpass scene. The thresholds are dynamic and satellite-specific. They are primarily based on simulations with Radiative Transfer Model (RTM) calculations. Validated against CloudSat/Cloud-Aerosol Lidar and Infrared Pathfinder Satellite Observation (CALIPSO) observations over the polar summer of 2007, the cloud mask showed a hit rate of 0.85 over the polar summer with a Kuiper's skill score of 0.62–0.67. The accuracy and validation of the Arctic cloud mask and other cloud products are discussed in detail in Karlsson and Dybbroe (2009).

2.1.2. Cloud mask update for sea ice

The cloud mask is updated with Ocean and Sea Ice Satellite Application Facility (OSI-SAF) sea ice concentration data (Breivik et al., 2001) to resolve any ambiguous sea ice pixels over the Arctic Ocean. The data source is the Special Sensor Microwave/Imager (SSM/I) on board the Defense Meteorological Satellite Program (DMSP) series of polar-orbiting satellites. The algorithm is based on a weighted combination of the Bristol (Smith, 1996) and Bootstrap (Comiso, 1986) algorithms. Both use pre-defined tie-in points to define open water and continuous ice, and then compare the ratios of the observed brightness temperatures to the tie-in points to derive the sea ice concentration. The OSI-SAF data is distributed at 10 km spatial resolution. Continuous sea ice concentrations in the Arctic Ocean are generally stable over a time period of one day, which is the OSI-SAF data update cycle. Thus the 10 km OSI-SAF resolution is assessed to be close enough to the ~1 km AVHRR resolution to cause minimal misclassifications, especially since the interest here is in identifying the continuous ice cover areas. Therefore, a threshold in the SAL algorithm is currently set to the value of 70% ice concentration to mark continuously ice-covered ocean. Discontinuous sea ice regions are not treated by the current algorithm. The ice-free water albedo is based on a look-up-table (Jin et al., 2004).

2.1.3. Atmospheric contribution

The TOA reflectances are reduced to surface reflectances by removing the atmospheric effects with the Simplified Method for Atmospheric Corrections (SMAC) algorithm by Rahman and Dedieu (1994). The SMAC algorithm performs a fast radiative transmission calculation based on the 6S radiation transfer model. The 6S model is based on the successive orders of scattering method, where the total reflected/scattered radiation from the atmosphere is calculated as a sum of the radiation intensities from the various orders of scattering in the atmosphere and reflection from the surface below. Atmosphere–surface coupling in the reflectance calculation is included. As input, it requires the observed TOA reflectances from the previous stage, the aerosol optical depth (AOD) at 550 nm, the columnar water vapour content of

the atmosphere in g/cm^2, the ozone content of the atmosphere in atm/cm^2, and the surface pressure in hPa.

In the current operational SAL processing, the water vapour and the surface pressure for each pixel are taken from Deutscher Wetterdienst (DWD) meteorological model data, whereas the ozone content is set to a constant of 0.35 atm/cm^2, and the AOD is set to a constant of 0.1. The DWD model, named GME (combination of global model (GM) and regional model (EM)), models the atmosphere using 60 layers (interpolated to 40 for SAL). It uses operational European Centre for Medium-Range Weather Forecasts (ECMWF) analysis products for initialising itself. The water vapour column content for SAL is operationally calculated by an integration of the separate layer water vapour contents. The retrievals presented here are computed slightly less accurately, as computational constraints forced the water vapour and surface pressure to be set at their default values of 2.5 g/cm^2 and 1013 hPa, respectively. The impact of these approximations in overall accuracy of the validation is expected to be of minor importance. The accuracy and limitations of the atmospheric correction are discussed further in Section 4.

2.1.4. Bidirectional Reflectance Distribution Function (BRDF) correction

We begin with a clarification of nomenclature. While the term 'BRDF correction' is widely used in the remote sensing community, the field measurements or satellite observations of electromagnetic radiative flux densities reflected by a surface actually provide only an approximation of the BRDF. The real BRDF of a surface is a ratio between the reflected radiation flux to an infinitesimal solid angle, and the incoming radiation flux from an infinitesimal solid angle. As such, it is a conceptual quantity (Schaepman-Strub et al., 2006). The accuracy of the BRDF approximation depends on how well the diffuse component of the incoming and reflected radiative flux densities can be removed with an atmospheric correction of the data or instrument set-up, and how small the observing instrument Instantaneous Field of View (IFOV) is. However, we choose to use the term 'BRDF correction' here to describe the process by which the satellite observations are compensated for their inability to observe the true bi-hemispherical reflectance, or surface albedo as it is commonly called, with a single measurement.

We postulate that a statistical BRDF correction can be achieved by temporally averaging albedo images without an individual BRDF correction. In our approach, a single overpass scene is not corrected for anisotropic reflection behaviour, because to our knowledge there are no universally valid snow BRDF models. The application of a model that does not fit the snow conditions would easily increase the retrieval error. Instead we choose to construct a statistical BRDF correction by temporally averaging all successful albedo retrievals over a given time period, here a week. Over the Arctic, there are between 177 and 244 overpasses available for each week in this study. Even accounting for culling of the data because of cloudiness and poor illumination/viewing geometries, at Summit GC-Net station between 8.5 and 16% of all overpasses per week in the validation period are successful albedo retrievals. Furthermore, Xiong et al. (2002) note that the BRDF correction may not be necessary for melting season conditions when the surface is a mix of snow and meltwater. They also state that the isotropy assumption will lead to albedo under- and overestimations of up to 20% over non-melting snow and ice, which is a prime reason why our goal is not to provide an albedo product that is accurate on the instantaneous level.

The angular reflective properties of snow at Summit have been studied by Bourgeois et al. (2006). They measured the hemispherical directional reflectance factor (HDRF) of snow, which has a similar behaviour to the bidirectional reflectance factor (BRF) of snow, except that the incoming radiation flux comes from the entire hemisphere. The BRF describes how much the reflected flux differs from one reflected from an ideal lambertian reflector. It is related to the actual BRDF by a factor of π (Schaepman-Strub et al., 2006). According to their results, the dry snow that is typical for Greenland and the Arctic region has a hemispherical directional reflectance factor (HDRF) clearly above lambertian reflectance in the forward scattering directions and clearly below lambertian reflectance in the backward-scattering directions. For rime-covered snow, the HDRF was reported to be fairly flat and close to lambertian reflectance for Sun zenith angles below 58°. The results by Peltoniemi et al. (2005) for boreal and subarctic snow show varying reflection behaviour depending on snow age, moisture content, and grain size. The resulting BRDF approximations support the postulation that snow reflectance behaviour changes significantly according to the ambient environmental state, as well as current and past physical properties of snow. Current optical satellite retrieval methods do not provide enough information on the physical properties of snow to choose an appropriate BRDF model for each case. But by sampling the scene on a sufficiently long time period, the cases where strong forward scattering or diminished backward scattering occurs could be compensated for if the amount of data is sufficiently high.

To provide evidence to support our approach, we show a distribution of Sun zenith angle (SZA) and viewing zenith angle (VZA) data for two week's worth of spatially and temporally matched overpasses at Summit station in Fig. 2. The period between July 9 and July 22 (days 190–203) contained 72 clear-sky overpasses. Fig. 2 shows the Sun zenith angles of these overpasses as a function of the viewing zenith angle of the satellite at Summit. Dark color circles correspond to overpasses where the azimuth difference between the Sun and the satellite was less than 90°, indicating backward scattering. Light color circles correspond to azimuth differences greater than 90°, indicating forward scattering. Therefore, it would seem plausible that temporal averaging of a symmetrical dataset of forward- and backward-direction albedo retrievals with an isotropic BRDF treatment would produce an estimate of the albedo fairly close to the actual hemispherically measured value. Xiong et al. (2002) compared near-nadir AVHRR overpasses without an anisotropy correction successfully with Surface Heat Budget of the Arctic Ocean (SHEBA) surface albedo observations with a similar methodology. Our approach expands the applicable viewing and illumination geometry range with the temporal averaging scheme.

Our sample dataset in Fig. 2 has 16 backward-direction retrievals to 56 forward-direction retrievals so the distribution is not even. However, for SZAs below 60°, both forward- and backward-scattering retrievals are evenly distributes in terms of the VZA, and their amounts are more balanced. This suggests that a higher degree of retrieval accuracy than shown in this study could be obtained if the retrievals were limited to below 60° SZA with our processing method. We calculate the weekly means of the successful albedo retrievals in this study to ascertain whether or not our proposed approach currently yields a comparable

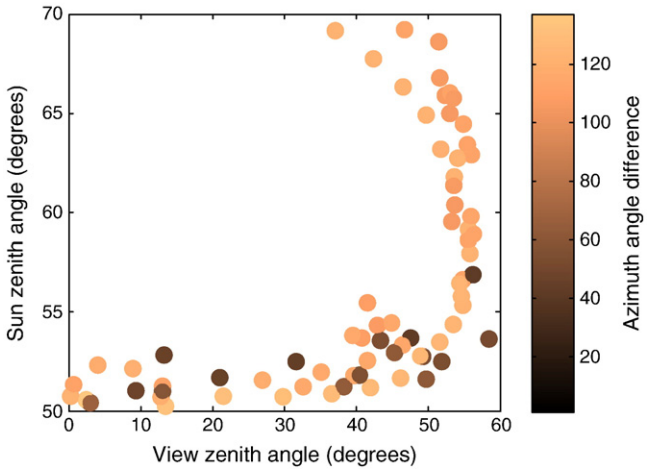

Fig. 2. Distribution of SZA and VZA angles of matched overpasses at Summit station between July 9 and July 22, 2007. Dark color corresponds to backward scattering, light color indicates forward scattering.

accuracy with other available Arctic satellite albedo datasets, such as the Polar Pathfinder (Wang & Key, 2004).

2.1.5. Conversion to broadband shortwave albedo and Sun Zenith Angle normalization

As the BRDF is accounted for by temporal averaging, we next apply the algorithm by Xiong et al. (2002) to obtain the surface broadband albedo estimate. This algorithm accounts for melt pond formation and should therefore be less prone to estimation errors during the melting season in the Arctic. The equation of the Narrow-To-Broadband (NTB) conversion is:

$$\alpha = 0.28(1 + 8.26\Gamma)\alpha_{RED} + 0.63(1-3.96\Gamma)\alpha_{NIR} + 0.22\Gamma-0.009 \quad (1)$$

where

$$\Gamma = \frac{\alpha_{RED}-\alpha_{NIR}}{\alpha_{RED} + \alpha_{NIR}}. \quad (2)$$

The conversion is an empirically derived combination of the spectral albedos, with a weighing factor Γ which compensates for the ponding and ice formation during melting season. As meltwater (or ice) forms on the snow, the NIR waveband albedo decreases more than on the red waveband because water absorbs radiation more strongly on the NIR waveband. This in turn increases the value of Γ, thus increasing the red waveband albedo but decreasing the NIR waveband albedo more strongly, resulting in a smaller broadband albedo. The accuracy of the NTB conversion is reported to be 5–10% (relative).

For any water pixels not covered by sea ice, the broadband albedo is retrieved from a look-up-table (LUT). The applied LUT is by Jin et al. (2004). The retrieved broadband ocean albedo depends on four parameters:

1. Sun zenith angle (SZA)
2. wind speed, SAL default = 10 m/s
3. aerosol optical depth (AOD), SAL default = 0.1
4. ocean chlorophyll content, SAL default = 0.15 mg/m^3.

At present, SAL processing has no access to realtime wind speed, AOD or chlorophyll content data, so default constants are used. Therefore the modeled ocean albedo depends in principle only on the SZA. However, since all distributed SAL products are normalized to a SZA of 60° (see below), all water pixels have in fact a constant broadband albedo value of 6.7%.

In this study, no Sun zenith angle normalizations are implemented. For discussion on the available options and implications on accuracy, the reader should see Section 4.

2.2. The validation dataset and methodology

2.2.1. Satellite data

The satellite dataset consists of 2755 AVHRR overpasses in the Arctic region, as illustrated in Fig. 1(b). This number includes only day-time overpasses, night-time overpasses before 05 UTC and after 22 UTC were not computed. All AVHRR retrievals corresponding to SZA>70° and VZA>60° were not computed. The surface albedo computation is not performed for any cloud-contaminated pixels over land or ocean.

2.2.2. In situ data — Greenland

The locations of the GC-Net stations used in this study are shown in Fig. 3 and listed in Table 1. The incoming and reflected radiative fluxes are measured with Kipp & Zonen CM-21 pyranometers at Summit and with LI-COR 200SZ photoelectric diode pyranometers at other GC-Net stations in this study. The data is provided as hourly averages from 15-s samples. The pyranometers are stabilized against strong wind, horizontally leveled and periodically maintained to ensure data quality. The limited spectral sensitivity (0.4–1.1 μm) of the LI-COR 200SZ is factory-adjusted to compensate for differences to full broadband sensitivity instruments, but a positive bias of approximately 0.04 has been reported (Steffen, 2009; Stroeve et al., 1997). The CM-21 has no reported bias, and it provides a close spectral match to the SAL product (0.305–2.8 μm).

Stroeve et al. (2005) reported that the LI-COR 200SZ measurement uncertainty is 5% for the downwelling shortware and 10% for the upwelling shortware flux. We did not attempt to adjust the GC-Net station albedo to account for any bias, since our goal is to show good retrieval accuracy in the temporal albedo means, where instantaneous corrections of station albedo would also require knowledge on the atmospheric state during the period. Stroeve et al. (2005) also stated that the residual LI-COR 200SZ measurement uncertainty had an RMSE of 0.035, and that any satellite retrieval errors exceeding that value would have noteworthy statistical significance. We use these values as a baseline for assessing SAL quality.

No data exists on the environmental changes experienced by the instruments such as frost formation or wind-induced leveling errors. The accumulation zone of the Greenland ice sheet is known to be quite stable, whereas the JAR-2 station near the edge of the ice sheet experiences changes of the surrounding ice sheet each year. As the summer progresses and surface temperature rises, the surface at JAR-2 changes from snow-covered ice to bare ice, and melt ponds form in July and August. The process is reversed at the freezeup phase in the autumn. The change in local surface conditions in the area observed by the LI-COR sensors can have a large effect on the recorded surface albedo in the cases of bare ice exposure and melt pond formation in the sensor footprint area, which is between 1.7 and 5.2 m^2 (Stroeve et al., 2006). Bare ice and melt ponds lower the surface-observed albedo considerably, while the satellite retrievals may not be similarly affected if the surface conditions of the overall station area do not match those at the pyranometer footprint. Therefore, care must be taken when assessing the retrieval accuracy in the ablation region. Conversely, as Summit station is permanently manned and the pyranometer regularly checked, and the environmental conditions are relatively stable, we expect to find there the highest degree of comparability between surface and satellite observations in this study.

2.2.3. In situ data — Ice-covered Arctic Ocean

Our validation period coincided with the Tara ship expedition to the Arctic Ocean. The French schooner Tara functioned as a drifting ice station between September 2006 and January 2008, the crew performing meteorological observations throughout the period (Gascard et al., 2008; Vihma et al., 2008). The route of the Tara is shown in Fig. 4, overlaid with an example IA-SAL overpass from July 17, 2007.

The upward and downward shortwave radiation fluxes were measured at Tara from 12 May to 19 September, 2007, applying Eppley PSP pyranometers. The sensors were set up at the height of 2 m above the snow surface. The pyranometers were cleaned and their horizontal alignment was checked every day by one of us (Timo Palo). The data were registered once a minute. The surface albedo was calculated as the ratio of the reflected and incoming shortwave radiation. On the basis of experience of application of similar pyranometers over snow-covered polar regions in summer (Schmidt & König-Langlo, 1994; Vihma et al., 2009), the accuracy of the shortwave radiation measurements was approximately 3%. This was confirmed by a post-expedition intercomparison of our pyranometers against those at the AWIPEV station in Ny Ålesund, Svalbard, which belongs to the Baseline Surface Radiation Network. Measuring albedo over highly reflecting surfaces like ice and snow, most of the errors associated with the accuracy of the upward and downward fluxes are compensated and, on the basis of the error calculations taking into account the solar zenith angle (Pirazzini, 2004), we estimated that the uncertainty in Tara albedo values was 2–4%.

In April and May the surface around Tara was snow-covered sea ice. The snow melt started on 10 June, i.e. two days before the first SAL

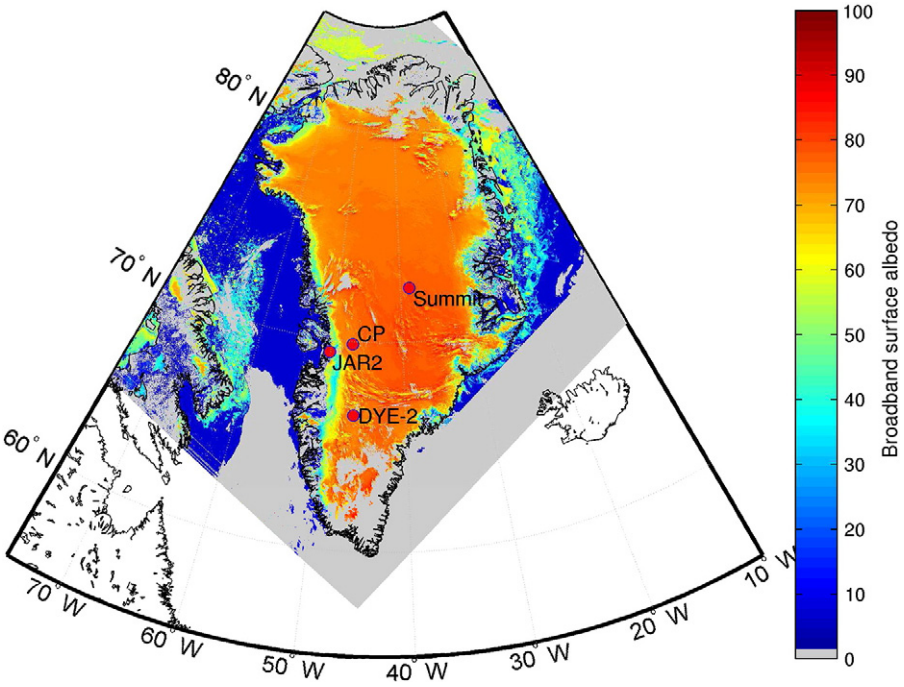

Fig. 3. Locations of the GC-Net stations used in the study overlaid with an example SAL overpass from July 10, 2007 at 15:35 UTC. Pixels masked with grey indicate cloud contamination or poor viewing/illumination geometry.

validation period. The melt first resulted in percolation of melt water to the snow–ice interface, but without formation of melt ponds. These started to appear on 22 June i.e. just before the end of the first SAL validation period. The melt–pond coverage increased from 3 to 14% between 24 and 30 June (Sankelo et al., in press; Nicolaus et al., 2010). From 4 to 6 July the surface drained in large scale, resulting in distinct melt ponds and drained areas of deteriorated, white sea ice (Nicolaus et al., 2010). There were four melt ponds close to the radiation sensors, the largest one next to pyranometers. On 21 July, in the end of the second SAL validation period, the fraction of melt ponds was 15% (Sankelo et al., in press), and during the third period from 28 July to 3 August the fraction was 25 to 30%.

The local surface conditions below the pyranometers were, however, somewhat different from the regional conditions described above. We observed that during the validation period, the local melt–pond fraction in a circle with 6-m radius under the pyranometers was on average 30%, whereas the regional melt pond fraction was on average 15%. The local surface was also artificially affected for a short period: To protect the radiation sensors from advancing melt ponds, on 30 June Timo Palo drilled a small hole through the ice, which drained the surface for a few days.

We did not observe other remarkable changes in the sea ice surface properties. The summer weather at Tara was characterized by air temperatures continuously close to 0 °C, low winds (2–6 m/s), and relative humidity almost continuously above 90%.

2.2.4. Methodology of the validation

The validation of a satellite-derived albedo dataset against in situ observations requires that the data must be matched spatially, temporally and spectrally. We perform spatial matching by seeking the ground-satellite observation pairs by a nearest-neighbor search. Naturally the coarse resolution of the AVHRR/3 instrument (1.09 km at nadir) causes the sampled areas to differ even during optimal conditions, i.e. homogeneous terrain for the in situ observation. However, we believe that the nature of the reference sites in Greenland

Table 1
The locations and elevations of the GC-Net stations used in this study.

Name	Latitude (N)	Longitude (E)	Elevation (m)
Summit	72.5794	−38.5042	3208
Crawford Point (CP)	69.8819	−46.9736	2022
DYE-2	66.4810	−46.2800	2165
JAR-2	69.4200	−50.0575	568

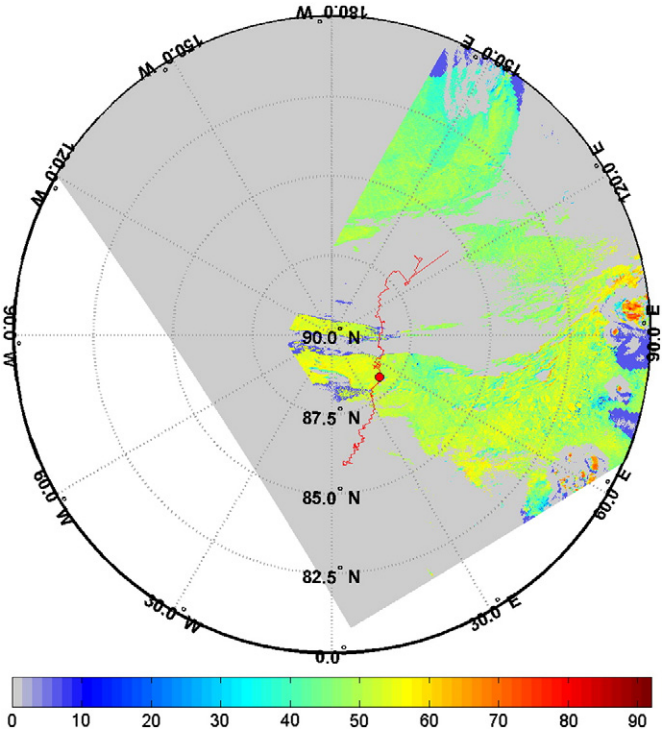

Fig. 4. Route of the Tara expedition (in red) used in the study overlaid with an example SAL overpass from July 17, 2007 at 7:53 UTC. Pixels masked with grey indicate cloud contamination or poor viewing/illumination geometry. Tara location at the time of overpass is marked by a red circle.

ameliorates this effect. The snow cover on the Greenland ice sheet is horizontally nearly homogeneous and most reference sites used in this study are located in the accumulation zone, where the snow experiences minimal melting. The lack of vegetation creates large, relatively uniform snow fields within which the precise location of the in situ observation point in relation to the positioning of the satellite pixel should not cause dramatic effects in accuracy. For example, the mean distance between the center of satellite pixel and the location of the Summit station where albedo observations are made was roughly 515 m for our dataset. This should be sufficiently small to ensure representability of the albedo observation for the larger area covered by the AVHRR pixel.

The validation over sea ice near the Tara schooner location is more prone to errors resulting from spatial mismatch due to the large physical variability of the Arctic sea ice and its snow cover (Weeks & Ackley, 1982).

Temporal matching of the satellite/in situ data pairs is straightforward at Tara because the in situ observations were made at 1-min intervals, ensuring direct comparability to SAL retrievals. The GC-Net station albedos are hourly averages from 15-s samples, thus their comparability to the instantaneous SAL data is dependent on the stability of the snow cover at the sites. Although rapid processes such as wind may alter the snow albedo, the studied station albedos are generally stable during intervals of one or a few hours. Thus, we choose not to attempt any adjustment of the data.

Spectral matching of the data involves no processing actions. The Eppley PSP pyranometer covers a waveband between 0.285 and 2.8 μm, which is close enough to the SAL waveband that the resulting albedo difference is negligible. The GC-Net pyranometers are Li-COR 200Z photoelectric diode pyranometers, which are spectrally sensitive between 0.4 and 1.1 μm. As mentioned before, this leads to a positive bias of around 0.04.

3. Validation results

3.1. GC-Net stations

Illustrations of the validation results from the GC-Net stations are shown in Figs. 5 and 6. Summaries of the instantaneous and weekly results are shown in Tables 2 and 3. The GC-Net stations located higher up on the ice sheet are shown in Fig. 5, the stations at or close to the ablation region on the west coast are shown in Fig. 6. The results show a low bias between SAL and station observations for the ice sheet stations despite significant variability in SAL due to the isotropic treatment for snow BRDF. At Summit, the mean station albedo over the whole three-month period was comparable to the SAL mean albedo over the same period, implying that the weekly and monthly SAL products may be accurately retrieved by averaging a temporally sampled retrieval set with varying illumination and viewing geometries. The standard deviation of the SAL dataset is higher than the Summit station dataset, since instantaneous SAL values are samples of empirical BRDF, whereas the ground measurements are hemispherically integrated albedos. Toward August, the station measurements begin to fluctuate, possibly due to the worsening illumination conditions toward the end of summer. The Sun zenith angles for successful matchings in August vary between 55 and 70°, but after August 16 the retrievals all occur at SZAs over 60°, with a mean of 63°. In addition to possible cosine correction difficulties and a greater vulnerability to leveling errors with these illumination conditions, the air temperatures begin to fall in August, causing increased rime formation on the pyranometer domes in the morning. Visual inspection of the data shows that most of the Summit datapoints showing an albedo over 0.9 in August are from morning hours, between 10 and 13 UTC. A slight increase in the variability of SAL may also be seen, although retrieved albedos below 0.65 occur at SZAs exceeding 60° and are thus likely misclassified clouds, or failed retrievals in challenging illumination conditions.

At DYE-2 the retrieval accuracy remains comparable to Summit (Fig. 5(b)). The difference between the mean station and SAL albedo is comparable to that at Summit. The dynamic range of retrieved albedos is similar, as the similar standard deviations suggest. As mentioned before, there is also a documented positive bias of about 0.04 in the GC-Net albedo measurements excepting Summit. If this were taken into account, the mean absolute difference between the weekly SAL albedo value and the DYE-2 albedo would be close to 0.007. The mean absolute difference at the weekly level is smaller than for the instantaneous retrieval comparisons. This further reinforces our postulation that fairly accurate time-averaged snow albedo products can be produced without an instantaneous BRDF correction. The retrieval accuracy of the temporal means of surface albedo with SAL appears to be on the same order of magnitude as the natural variability of albedo over the Greenland glacier. The RMSE of both Summit and DYE-2 is on the same order of magnitude as the residual station albedo RMSE given by Stroeve et al. (2005).

Over the ablation region on the west coast of Greenland, we expect to find lower retrieval accuracy due to changing snow surface heterogeneity between the satellite pixel and pyranometer footprint (i.e. different fractions of dirty snow, bare ice exposure, or melt ponds). The formation of large crevasses may also affect satellite retrievals, but the crevasses cannot be identified from the imagery. Also, there are slopes of 1–5° present in the area around JAR-2 station according to the Advanced Spaceborne Thermal Emission and Reflection Radiometer (ASTER) Global Digital Elevation Model (GDEM) (Hato et al., 2009). These slopes may have a minor effect on the retrieved satellite albedo. The results in Fig. 6(a) show that SAL has a tendency to overestimate the surface albedo at JAR-2 station. The difference is on average approximately 0.13, although over-estimations up to 0.3 occur. Stroeve et al. (2001) reported higher discrepancies between the AVHRR Polar Pathfinder (APP) dataset and station observations over the ablation region, but the APP algorithm underestimated the in situ albedo. Interestingly, Stroeve et al. (2005) also reported an overestimation of observed albedo by MODIS at JAR-2, in the same manner as SAL in this study, although their bias was considerably smaller.

It should be kept in mind that the both the Greenland ice sheet and the Arctic Ocean sea ice cover experienced significantly more melt in 2007 than the climatological averages (Comiso et al., 2008; Mote, 2007). The melting season was longer and melting occurred at higher elevations than normally. It is highly likely that the JAR-2 station pyranometers observed melt ponds and bare ice for long periods over the summer. Thus the station albedos are expected to be significantly lower in this study than in previous ones. This can lead to higher discrepancies in our comparison, if the large area fraction of melt ponds and bare ice is not the same as in the pyranometer footprint. Naturally, the coarse spatial and spectral resolution of AVHRR compared to MODIS also sets limitations on accuracy, regardless of surface conditions. It is clear that the coastal zone of Greenland is a highly challenging region for satellite-based retrievals of surface albedo. The next version of SAL will include a topography correction, which the authors hope will ameliorate the retrieval inaccuracies particularly over the steeply sloped east coast of Greenland.

Over Crawford Point (CP), we find that SAL underestimates the station observations by about 0.1 on average. The CP station albedo, like that at DYE-2 shows higher variance than Summit because the environmental conditions are not so stable. The observed in situ albedo is in line with Stroeve et al. (2001), but slightly higher than the values shown in Stroeve et al. (2005). This suggests that CP station albedo has naturally a high variance that accounts for the results seen in this study.

When we compare the data between Tables 2 and 3, we find that the bias and RMSE of the weekly products are smaller in nearly all locations. This is in line with our expectations since the temporal averaging is necessary for our BRDF sampling strategy.

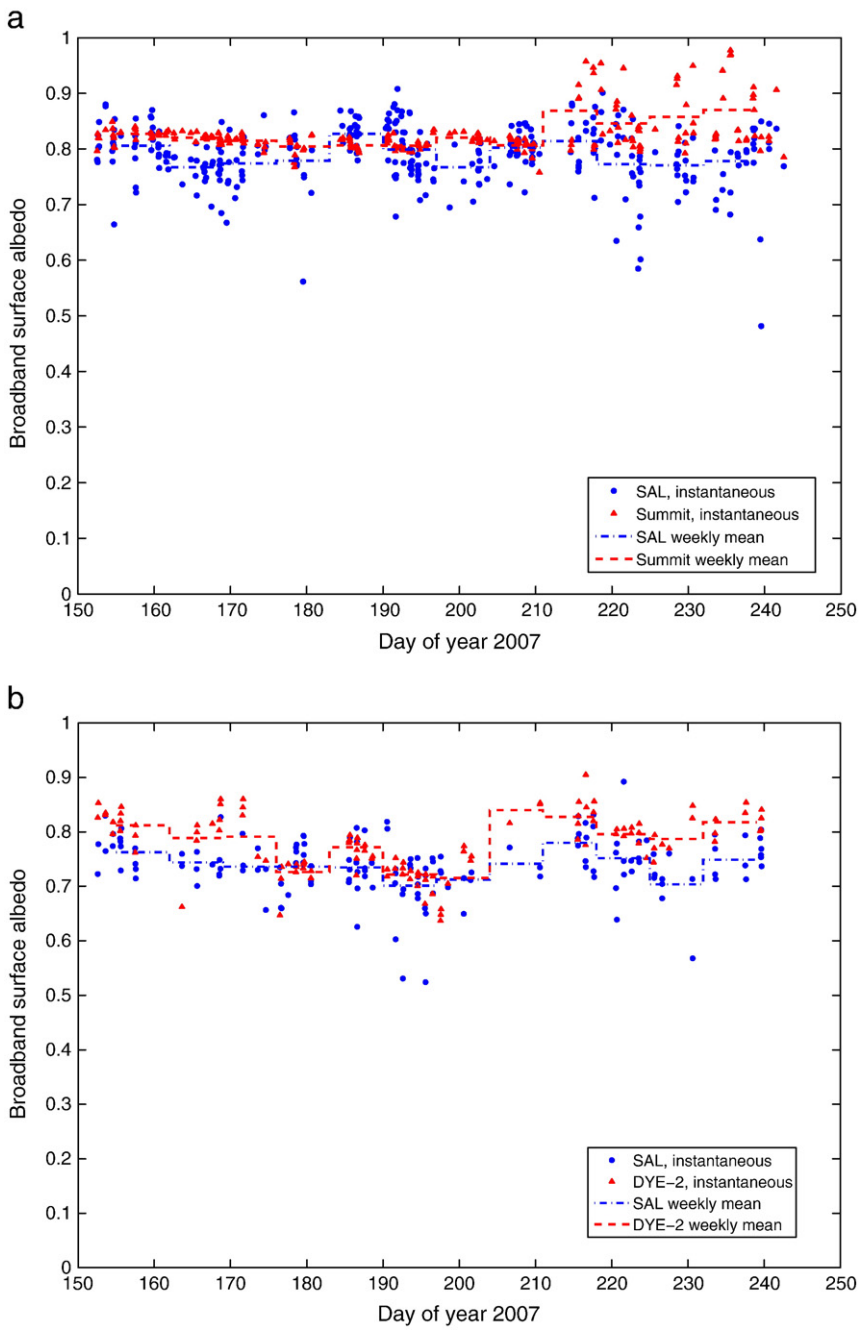

Fig. 5. The validation results from GC-Net stations on the glacier. (a) Comparison between SAL retrievals over Summit station and locally measured broadband albedo. Time period: June 1 - August 31, 2007. (b) Comparison between SAL retrievals over DYE-2 station and locally measured broadbandalbedo. Time period: June 1 - August 31, 2007.

3.2. Ice-covered Arctic Ocean

The second part of this validation is concerned with the performance of SAL over the Arctic sea ice. The results of the validation of SAL against Tara ice station albedo observations are shown in Fig. 7. The overall quality of SAL retrievals appears to be fairly good, although the number of clear-sky overpasses is quite small due to the almost persistent cloud cover over the Arctic Ocean in summer. The mean difference between SAL retrievals and local albedo observations is quite comparable to GC-Net station validation. In early summer the natural variability of sea ice albedo is on the same order of magnitude as the variation of SAL. During mid-summer (days 196–214), the natural variability of in situ data is very large, as also shown also by Vihma et al. (2008). Much if the variability is related to the temporal evolution of melt ponds in the vicinity of the radiation sensors (see Section 2.2.3). With increasing snow melt from 12 to 23 June, the SAL albedo value decreased (Fig. 7), with the low value of 0.55 detected at the time when we observed the first melt ponds at Tara. The higher SAL value observed on 30 June is related to snow fall and slight refreezing of melt ponds. During the later validation period (Julian days 196–214), the surface close to Tara was ponded, both in large scale and even more below the pyranometers (see Section 4.) During the later validation period (Julian days 196–214), the surface close to Tara was ponded. Although the in situ measurements were slightly affected by the local melt ponds, the shift to predominantly lower SAL than in situ albedo values may be related to a smaller melt pond fraction in the immediate vicinity of the radiation sensors than in the SAL pixel on average.

SAL appears capable of following the negative seasonal trend in the albedo of sea ice as the summer progresses. To see whether or not the low number of matched overpasses creates a misrepresentation of

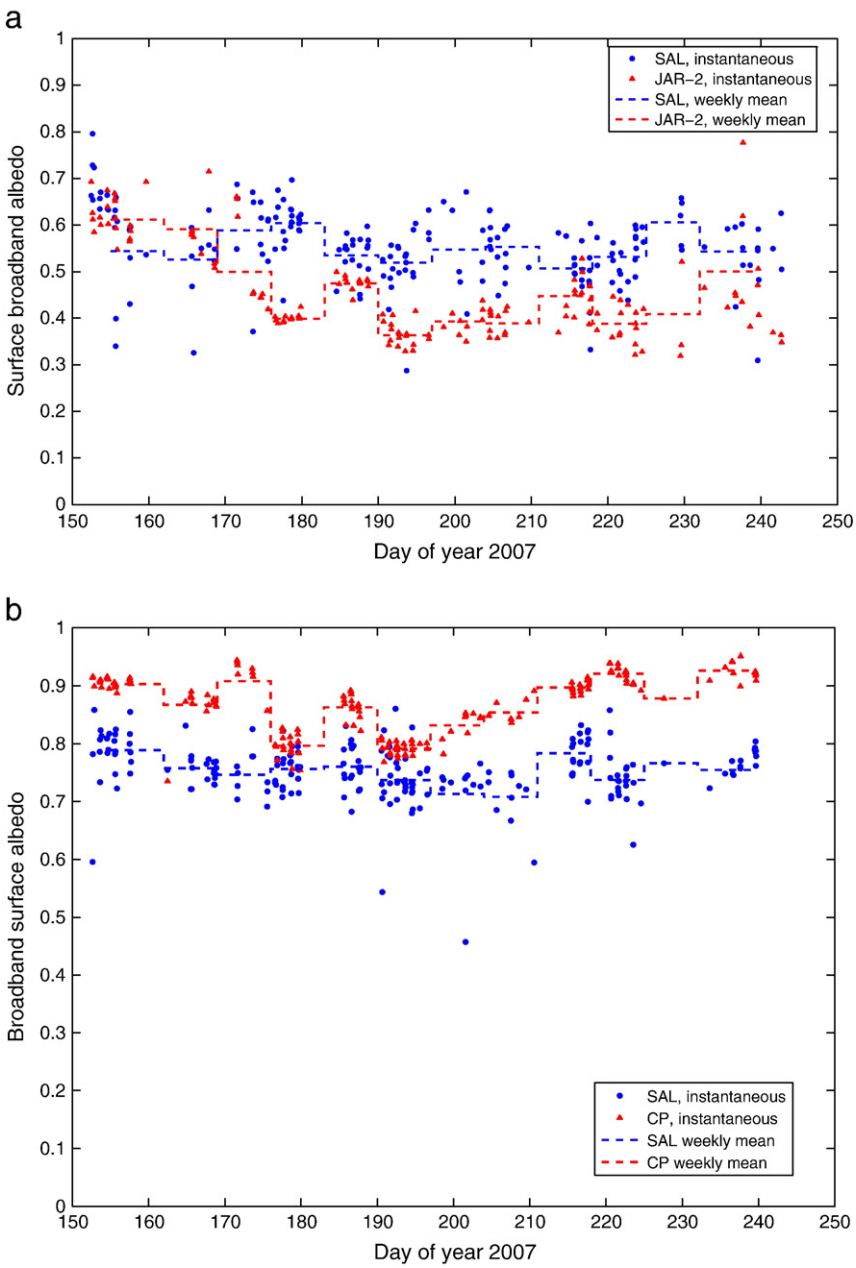

Fig. 6. The validation results from GC-Net stations at or near the ablation region. (a) Comparison between SAL retrievals over JAR-2 station and locally measured broadbandalbedo. Time period: June 1 - August 31, 2007. (b) Comparison between SAL retrievals over Crawford Point station and locally measuredbroadband albedo. Time period: June 1 - August 31, 2007.

retrieval accuracy, we also performed the analysis allowing a maximum distance of 1500 m between the Tara location and the nearest SAL pixel center. After removing misclassified retrievals, N increases to 56 and RMSE of the individual overpasses remains fairly constant at 0.064. This shows that SAL retrievals are stable, except where cloud misclassifications occur. To test the statistical hypothesis that the observed SAL values are statistically not significantly different from the observed in situ albedo values, we performed a paired Student's t test on the original

Table 2
Summary of the validation results of instantaneous SAL albedo values versus GC-Net station and Tara observations. Time period: June 1–August 31, 2007.

Station	Station mean	SAL mean	Mean of abs. differences	Station stdev	SAL stdev	RMSE	N
Summit	0.825	0.790	0.053	0.036	0.053	0.073	336
DYE-2	0.774	0.738	0.057	0.052	0.052	0.073	153
JAR-2	0.453	0.553	0.130	0.097	0.078	0.151	195
CP	0.862	0.754	0.110	0.053	0.048	0.126	222
Tara	0.578	0.552	0.053	0.084	0.074	0.069	39

Table 3
Weekly mean SAL albedo values compared against weekly means of GC-Net station and Tara observations. Time period: June 1–August 31, 2007.

Station	Mean abs. difference In weekly means	Max abs. difference	RMSE	N (weeks)
Summit	0.044	0.092	0.053	12
DYE-2	0.047	0.099	0.054	12
JAR-2	0.117	0.206	0.130	12
CP	0.120	0.184	0.126	12
Tara	0.038	0.070	0.045	6

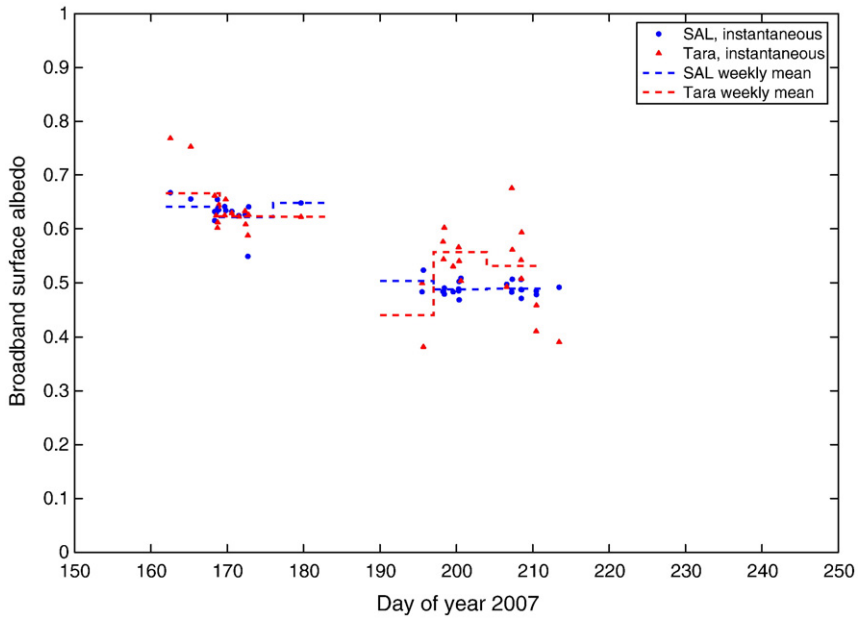

Fig. 7. Validation results from the Tara ice station between June 1 and August 31, 2007. SAL retrievals marked with blue circles, corresponding Tara observations with red circles. Weekly means marked with blue (SAL) and red (Tara) where available.

39 matched overpasses. The resulting t score of 2.58 shows that the SAL retrievals are statistically different at the 95% confidence level. The issues of melt pond effects and atmospheric contribution affect data comparability, which will be discussed in Section 4.1. The effect of the OSI-SAF ice concentration data gap above 88 °N is included in the considerations of Section 4.

3.3. Uncertainty analysis of satellite retrievals

When we consider the reliability of this validation study, we need to assess the uncertainty of SAL retrievals. The main sources of retrieval uncertainty for SAL are:

- cloud masking and cloud shadows
- shadowing effects caused by topography
- isotropic BRDF treatment
- narrow-to-broadband (NTB) conversion inaccuracy
- atmospheric correction errors
- shadowing effects due to large-scale surface roughness (ridges up to 2 m high near Tara).

To assess the impact of various error sources on broadband albedo retrieval accuracy, we will re-examine the Summit SAL retrievals. Because the delineation of clouds and snow is challenging, cloud masking may occasionally produce a misclassification of clouds as snow. While the error in instantaneous albedo may be large, over the validation we observed a likely misclassification in less than 2% of all matched retrievals. Xiong et al. (2002) states that the NTB conversion uncertainty is generally between 5 and 10% (relative). We then note that since the environmental conditions at Summit remain stable throughout the year (Ohmura, 2001), the SMAC atmospheric correction algorithm in SAL contributes very little to instantaneous SAL variability since its main inputs are also constants. Furthermore, as Summit is located on a large, even plateau, topography effects in the albedo retrievals are negligible. Thus, variability above 5–10% in instantaneous SAL retrievals over Summit is statistically significant and expected to result from the BRDF approach as long as the environmental conditions may be assumed to remain constant.

The albedo at Summit is stable between days 150 and 210 (standard deviation of 0.013). Removing the retrievals in poor illumination conditions (SZA over 65°) or suspicion of cloud contamination, there are 208 overpasses in this period with a mean absolute difference between station and SAL retrievals of 0.039 with a standard deviation of 0.031. Maximum discrepancy is 0.148. In relative terms, the mean absolute difference is 4.85% of the mean Summit albedo of this time period. There are 20 overpasses out of the 208 where the difference exceeds 10%, signifying that a relatively small number of the SAL retrievals is severely affected by the isotropic treatment. Of the cases with higher errors, the majority occurred with satellite zenith angles above 30°. In terms of Sun zenith angle, the higher error cases occurred at all angles between 50 and 70°. In terms of relative azimuth angles, overestimations mostly occurred at angles above 100° when forward scattering behaviour of snow dominated the satellite-observed reflectance, and underestimations occurred at both forward- and backward-scattering cases. The weekly mean of the retrieval error is between 4 and 7%, implying that the empirical temporal BRDF sampling strategy does not cause a statistically significant error in the weekly mean product. The retrieval errors for the overpasses and their weekly mean between days 150 and 210 are shown in Fig. 8.

The atmospheric correction error is difficult to quantify because no on site measurements of atmospheric AOD, ozone or water vapour content exist from the validation period at the GC-Net stations. As previously discussed, our assumed AOD of 0.1 is in fairly good agreement with values reported by Stroeve et al. (1997). The other major input in the SMAC calculations is water vapour content in the atmosphere. Resource constraints forced the use of processing default value of 2.5 g/cm^2 in this study. The Climate-SAF column water vapour product generated from ATOVS data (Schulz et al., 2009) shows that an appropriate value for the water vapour content over central Greenland in early summer 2007 is 0.5–1 g/cm^2. On the other hand, according to the ERA-40 reanalyses of the European Centre for Medium-Range Weather Prediction (ECMWF), the value of 2.5 g/cm^2 well represents the mean conditions in the study region in early summer (Jakobson & Vihma, 2009). In any case, the sensitivity of the SAL results to the column water vapour was small. Simulations using a copy of the SMAC code used in SAL show that the difference in the atmospheric correction using the default value of 2.5 g/cm^2 and 1 g/cm^2 is on the order of 1–1.5% for snow albedos ranging from 0.75 to 0.9. Stroeve et al. (1997) studied the sensitivity of satellite-derived

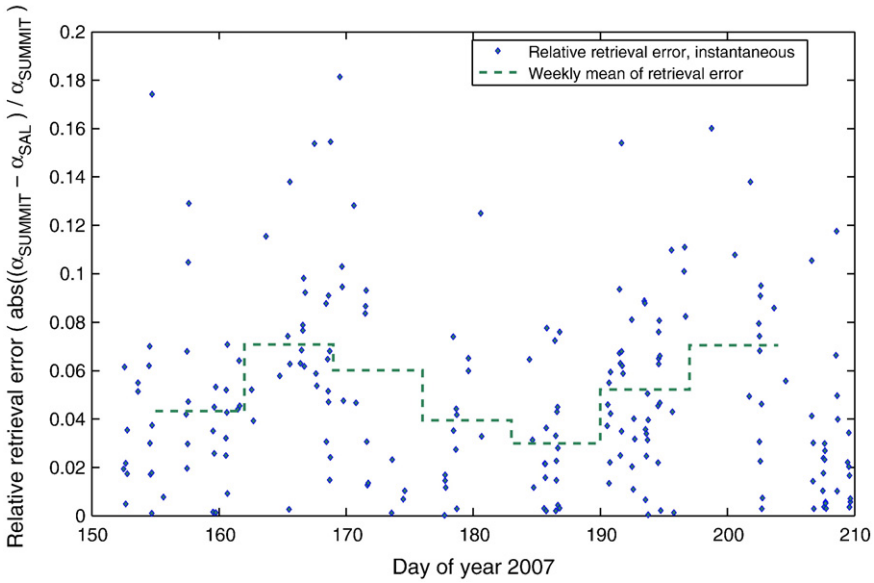

Fig. 8. Retrieval error at Summit between day 150 and day 210 of 2007.

surface albedo to inaccuracies in atmospheric state knowledge. They found that 20% relative error in water vapour content resulted in just a 0.15% relative error in surface albedo. The water vapour content input may therefore be seen as of minor importance. As mentioned before, operational SAL products employ Deutscher Wetterdienst model data for the water vapour and surface pressure inputs and should actually therefore be slightly more accurate than the retrievals shown here.

4. Discussion

4.1. Measurement comparability

The literature on albedo retrievals and retrieval validation indicates a need to distinguish between inherent (black-sky) and apparent (blue-sky) albedo retrievals and their comparisons (Lewis & Barnsley, 1994; Schaaf et al., 2002). SAL is an inherent albedo product, where the atmospheric contribution is removed. The pyranometers on the ground at our validation locations measure the apparent albedo, where the atmospheric contribution is dynamic. This places some limits on the comparability of SAL retrievals to the in situ observations, but we believe that the study approach is still valid. SAL is only computed for confirmed clear-sky situations, within the accuracy of the cloud mask. In these clear-sky situations at Arctic latitudes, previous studies have shown that the atmosphere is typically optically thin, and quite dry over the Greenland ice sheet (see previous section). Key (2002, Fig. 1) shows some radiative transfer simulation results on the differences of inherent and apparent albedo for high and low AOD and water vapour conditions in the atmosphere at a wide range of SZA. The results show that for a dry, optically thin atmosphere we may expect a difference of 0.02–0.05 between inherent and apparent albedos for SZA not exceeding 70°. While this is certainly a noteworthy difference, the other uncertainties in the satellite albedo retrieval and in situ observations are on the same order of magnitude. Thus this effect will not dominate the evaluation of the albedo retrieval accuracy.

Another aspect in the uncertainty analysis is that the in situ measurements and SAL data do not represent exactly the same region. The in situ measurements are point measurements. Using a downward-looking Eppley PSP pyranometer deployed at the height of 2 m, 50% of the reflected radiation originates from a circle with a 2 m radius, and 90% originates from a circle with a 6-m radius. The LI-COR and Kipp & Zonen pyranometers used at GC-Net stations have similar or smaller footprints. The SAL product represents the albedo of an area of at least 1.19 km^2. In the case of Tara measurements, the sea ice concentration in the vicinity of the radiation sensors was always 100% but the melt pond fraction varied. The larger melt–pond fraction below the pyranometers than in the satellite pixel (see Section 2.2.3) generates uncertainty in the comparisons. We can estimate this uncertainty by assuming a mean albedo of 0.6 for melting snow (Fig. 7) and 0.45 for melt ponds (Perovich et al., 2002). As the mean melt pond fraction below the pyranometers was 0.3 and at the SAL pixel 0.15, we get an estimate that the different melt pond fraction generates an error of 0.02 in the in situ–SAL comparison, which is of the same order of magnitude than the inaccuracy of the in situ measurements. Taking into account both error sources, we conclude that SAL agrees with in situ observations within their limits of accuracy and spatial representativeness.

We estimate the open water fraction around Tara to be 5% during June, as there were very few observed open water leads. During July, the ice became more dynamic and the open water fraction grew to 20% at the end of the month. This has no direct effect on the in situ observations, but could affect SAL retrievals. We have no means of estimating the fraction of open water at each individual SAL retrieval shown in Fig. 7, but the fact that SAL retrievals remained very stable during the days 196 and 214 suggests that increasing open water fraction was not a major source of uncertainty. The employed NTBC algorithm (Xiong et al., 2002) compensates for lower NIR albedos resulting from areas where water is mixed with snow and ice.

4.2. Sea ice

The current SAL algorithm processes sea ice albedo for continuous sea ice fields with ice concentration above 70%. Since the ocean albedo is LUT-based, the overall Arctic Ocean albedo would be more accurate if the discontinuous sea ice region would be included in the sea ice albedo algorithm. We are considering a linear combination of ice-free ocean and ice albedo algorithms to generate the Polar ocean albedo according to observed ice concentrations in a future update to resolve this issue, in accordance to the approach adopted in the Polar Pathfinder dataset (Scambos et al., 2002). Because the OSI-SAF Northern Hemisphere sea ice extent product is computed using independent microwave satellite observations, it also provides an excellent data source for verifying the cloud/ice-delineation in the cloud mask. However, above 88°N the OSI-SAF ice concentration product is not defined, therefore cloud mask misclassifications may

affect retrievals. The effect on the weekly and monthly products is minor, but the issue has been noted and means of rectifying it are being evaluated.

The OSI-SAF products are distributed in 10 km spatial resolution. While coarser than AVHRR resolution, there are currently visible effects only at AVHRR pixels at or next to coastlines where masking is applied to prevent misclassifications. Over the Arctic Ocean, any misclassification effect resulting from classifying AVHRR pixels according to the coarser resolution OSI-SAF data is smoothed out when the end product is resampled to 15×15 km spatial resolution for distribution.

4.3. Atmospheric correction

The current version of SAL uses constants for ozone content and AOD in the atmosphere. The best possible accuracy for the atmospheric correction would demand that both ozone and AOD be calculated on-line for each individual overpass. However, we wish to point out that the AOD for Arctic latitudes is most likely small; authors such as Curry et al. (1996) characterize the Arctic aerosol concentrations as being small and of secondary importance to the surface radiation budget. Field measurements by Stroeve et al. (1997) at ETH/CU station in West Greenland gave AOD values of 0.05–0.1, therefore our assumption seems adequate for now. It is noteworthy that to date there are no long time series of satellite-based Arctic AOD data because of the difficulties involved in retrieving AOD over very bright snow and ice surfaces in the Arctic regions.

4.4. BRDF

In the older SAL versions, BRDF correction of the snow surface reflectance is computed by using the algorithm of Manalo-Smith et al. (1998). However, Lubin and Weber (1995) questioned the use of ERBE-based angular dependency models in the use of BRDF corrections for AVHRR channel reflectances. As we further note that the Manalo-Smith algorithm was intended for use at the TOA level and not at the Earth surface, we find that the atmospheric contribution will also contribute to the retrieval error. Therefore we have chosen to change our approach to a temporal sampling of the BRDF at the end product level, as explained previously.

4.5. SZA normalization

In previous SAL versions, the dependence of albedo from Sun zenith angle was accounted for following an approach after the works of Dickinson (1983) and Briegleb et al. (1986) to normalize the products to a constant SZA. With recent studies into the diurnal cycle of snow albedo, we observed that the SZA dependence of snow albedo may not be treated with a noon-symmetrical U-shaped correction, which is appropriate for snow-free vegetated surfaces. The day-time clear-sky snow albedo typically decreases monotonously as the day progresses (McGuffie & Henderson-Sellers, 1985; Pirazzini, 2004). Thus, to normalize the albedo to a particular SZA one would need to know the rate of albedo decrease as well as choose whether to normalize to morning or afternoon occurrence of the 60° Sun zenith. Since the driving factors of snow albedo decrease during its diurnal cycle are quite complex and their study remains ongoing, the authors have decided to complete this study without any SZA normalizations in either satellite retrievals or in situ observations. The future SAL snow and ice albedo products will also not contain a SZA normalization routine until a robust method of dealing with the varying diurnal cycle of snow albedo has been developed.

5. Conclusions

This paper presents the results of a validation study undertaken to ascertain the quality of the new CM-SAF Arctic surface broadband albedo product (SAL). For the validation period, summer 2007, we performed an analysis of 2755 AVHRR overpasses to match the satellite data temporally, spatially and spectrally against in situ measurements of surface albedo taken in various automated Greenland Climate Network weather stations and at the drifting ice station of the Tara expedition. Satellite albedo images were processed with the procedures of the operational SAL product generation, including cloud masking, ice mask inclusion, atmospheric correction using SMAC, and narrow-to-broad-band conversion. Anisotropic effects of snow reflectance were treated with temporal sampling of illumination–viewing geometries and averaging because robust, universally applicable snow BRDF model for AVHRR was not available. Also, resource and time constraints forced some compromises in the atmospheric correction processing of the AVHRR data.

The results show that SAL is able to generate time-averaged products with an accuracy of 5–10%, even though the instantaneous differences from in situ measurements are sometimes larger. The retrieval accuracy appears similar for both snow over land and snow over sea ice, although the Tara data are quite sparse because of the almost persistent cloud cover at the highest latitudes. Taking into account the inaccuracy in the local albedo measurements at Tara and the effect of melt ponds, we conclude that SAL agrees with in situ observations within their limits of accuracy and spatial representativeness.

The satellite-based snow albedo becomes at times under- or overestimated when no instantaneous BRDF correction is applied, but an average of the instantaneous overpasses over a sufficiently long period can provide a good estimate of the albedo by temporal sampling of the BRDF. In comparison to similar studies conducted using APP dataset such as by Stroeve et al. (2001), SAL appears capable of performing at the same level in the weekly products. Areas with steep topographic changes such as the Greenland east coast, or rapid environmental changes such as the Greenland west coast, are problematic. Further improvements in the processing steps may increase our performance in such areas, but evidence from studies with higher-resolution sensors such as MODIS (Stroeve et al., 2005) point to the need for high spatial resolution, sophisticated BRDF models and topography effect compensation as necessary qualifications for accurate albedo retrieval with satellites over such terrain.

The Arctic SAL product covers land, ocean and sea ice albedo over the high latitudes. The algorithm remains under development. Future planned improvements include a topography correction for the satellite radiances as well as a function to compute the surface albedo over areas with non-continuous sea ice cover. Currently the sea ice albedo retrieval handles only regions of continuous sea ice (over 70% concentration). Albedo of low-concentration sea ice is being studied for inclusion into the algorithm.

Acknowledgements

This study has been financially supported by the Climate-SAF project of EUMETSAT, the EC 6th Framework Project DAMOCLES and the Academy of Finland through the project SAARA (#128261). The authors would like to thank Prof. Konrad Steffen and his research group at the University of Colorado for the Greenland Climate Network data. Frank Kaspar and Nathalie Selbach of DWD are thanked for their valuable support in the data processing. Erko Jakobson and Marcel Nicolaus are acknowledged for their contributions to Tara measurements. The two anonymous reviewers are thanked for their helpful comments and suggestions.

References

Bourgeois, C. S., Calanca, P., & Ohmura, A. (2006). A field study of the hemispherical directional reflectance factor and spectral albedo of dry snow. *Journal of Geophysical Research*, D20108.

Breivik, L. -A., Eastwood, S., Godøy, Ø., Schyberg, H., Andersen, S., & Tonboe, R. (2001). Sea ice products for EUMETSAT satellite application facility. *Canadian Journal of Remote Sensing*, 403−410.

Briegleb, B., Minnis, P., Ramanathan, V., & Harrison, E. (1986). Comparison of regional clear-sky albedos inferred from satellite observations and model computations. *Journal of Climate and Applied Meteorology*, *25*, 214−226.
Comiso, J. (1986). Characteristics of Arctic Sea ice from satellite multispectral microwave observations. *Journal of Geophysical Research*, 975−994.
Comiso, J. (2001). Satellite-observed variability and trend in sea-ice extent, surface temperature, albedo and clouds in the Arctic. *Annals of Glaciology*, 457−473.
Comiso, J. C., Parkinson, C. L., Gersten, R., & Stock, L. (2008). Accelerated decline in the Arctic Sea ice cover. *Geophysical Research Letters*, L01703.
Curry, J. A., Rossow, W. B., Randall, D., & Schramm, J. L. (1996). Overview of Arctic cloud and radiation characteristics. *Journal of Climate*, 1731−1764.
DeAbreu, R., Key, J., Maslanik, J., Serreze, M., & LeDrew, E. (1994). Comparison of in situ and AVHRR-derived broadband albedo over Arctic Sea ice. *Arctic*, *47*, 288−297.
Dickinson, R. E. (1983). Land surfaces processes and climate − Surface albedos and energy balance. *Advances in Geophysics*, 305−353.
Dybbroe, A., Thoss, A., & Karlsson, K. G. (2005). SAFNWC AVHRR cloud detection and analysis using dynamic thresholds and radiative transfer modelling part I: Algorithm description. *Journal of Applied Meteorology*, 39−54.
Gascard, J. -C., Bruemmer, B., Offermann, M., Doble, M., Wadhams, P., Forsberg, R., et al. (2008). Exploring Arctic transpolar drift during dramatic sea ice retreat. *EOS*, *89*, 21−28.
Hato, M., Tsu, H., Tachikawa, T., Abrams, M., & Bailey, B. (2009). The ASTER global digital elevation model (GDEM) − For societal benefit. *AGU Fall Meeting Abstracts*, B65+.
Holland, M. M., & Bitz, C. (2003). Polar amplification of climate change in coupled models. *Climate Dynamics*, 221−232.
Jakobson, E., & Vihma, T. (2009). Atmospheric moisture budget over the Arctic on the basis of the ERA-40 reanalysis. *International Journal of Climatology*. doi:10.1002/joc.20392009
Jin, Z., Charlock, T. P., Smith, W. L., Jr, & Rutledge, K. (2004). A parameterization of ocean surface albedo. *Geophysical Research Letters*, L22301.
Karlsson, K. -G., & Dybbroe, A. (2009). Evaluation of Arctic cloud products from the EUMETSAT climate monitoring satellite application facility based on CALIPSO–CALIOP observations. *Atmospheric Chemistry and Physics Discussions*, *9*, 16755−16810.
Key, J. R. (2002). *The Cloud and Surface Parameter Retrieval (CASPR) System for Polar AVHRR, User's Guide, part 2: Reference*. Technical Report NOAA/NESDIS/ORA/ARAD/ASPT.
Key, J. R., Wang, X., Stoeve, J. C., & Fowler, C. (2001). Estimating the cloudy-sky albedo of sea ice and snow from space. *Journal of Geophysical Research*, 12489−12497.
Knap, W. H., & Oerlemans, J. (1996). The surface albedo of the Greenland ice sheet: Satellite-derived and in situ measurements in the Søndre Strømfjord area during the 1991 melt season. *Journal of Glaciology*, 364−374.
Laine, V. (2004). Arctic sea ice regional albedo variability and trends, 1982–1998. *Journal of Geophysical Research*, *C06027*. doi:10.1029/2003JC001818
Lewis, P., & Barnsley, M. J. (1994). *Influence of sky radiance distribution of various formulations of the earth surface albedo.* Proceedings of the 6th International Symposium on Physical Measurements and Signatures in Remote Sensing. France: Val d'Isere.
Liang, S., Stroeve, J., & Box, J. E. (2005). Mapping daily snow/ice shortwave broadband albedo from moderate resolution imaging spectroradiometer (MODIS): The improved direct retrieval algorithm and validation with Greenland in situ measurement. *Journal of Geophysical Research*. doi:10.1029/2004JD005493
Lindsay, R. W., & Rothrock, D. (1994). Arctic sea ice albedo from AVHRR. *Journal of Climate*, 1737−1749.
Lubin, D., & Weber, P. G. (1995). The use of cloud reflectance functions with satellite data for surface radiation budget estimation. *Journal of Applied Meteorology*, 1333−1347.
Manabe, S., & Stouffer, R. (1980). Sensitivity of a global climate model to an increase of CO_2 concentration in the atmosphere. *Journal of Geophysical Research*, 5529−5554.
Manalo-Smith, N., Smith, G., Tiwari, S., & Staylor, W. (1998). Analytic forms of bidirectional reflectance functions for application to earth radiation budget studies. *Journal of Geophysical Research*, 19733−19752.
McGuffie, K., & Henderson-Sellers, A. (1985). The diurnal hysteresis of snow albedo. *Journal of Glaciology*, 188−189.
Moritz, R. E., Bitz, C. M., & Steig, E. J. (2002). Dynamics of recent climate change in the Arctic. *Science*, *298*, 1497−1502.
Mote, T. L. (2007). Greenland surface melt trends 1973–2007: Evidence of a large increase in 2007. *Geophysical Research Letters*, L22507.
Nicolaus, M., Gerland, S., Hudson, S., Hanson, S., Haapala, J., & Perovich, D. (2010). Seasonality of spectral albedo and transmittance as observed in the Arctic transpolar drift in 2007. *J. Geophys. Res*. doi:10.1029/2009JC006074
Ohmura, A. (2001). Summit Greenland environment observatory (report).*Memoirs of National Institute of Polar Research*, *54*, 153−159 Special issue.
Peltoniemi, J., Kaasalainen, S., Naranen, J., Matikainen, L., & Piironen, J. (2005). Measurement of directional and spectral signatures of light reflectance by snow. *IEEE Transactions on Geoscience and Remote Sensing*, *43*, 2294−2304.
Perovich, D., Grenfell, T., Light, B., & Hobbs, P. (2002). Seasonal evolution of the albedo of multiyear Arctic Sea ice. *Journal of Geophysical Research*, 1−13.
Perovich, D., Nghiem, S., Markus, T., & Schweiger, A. (2007). Seasonal evolution and interannual variability of the local solar energy absorbed by the Arctic Sea ice–ocean system. *Journal of Geophysical Research*. doi:10.1029/2006JC003558
Pirazzini, R. (2004). Surface albedo measurements over Antarctic sites in summer. *Journal of Geophysical Research*, D20118.
Rahman, H., & Dedieu, G. (1994). SMAC: A simplified method for the atmospheric correction of satellite measurements in the solar spectrum. *International Journal of Remote Sensing*, 15.
Sankelo, P., Rinne, E., Haapala, J., & Heiler, I. (in press). Melt pond formation and temporal evolution at drifting station *Tara* during summer 2007. *Polar Research*. doi:10.1111/j.1751-8369.2010.00161.x
Scambos, T., Haran, T., Fowler, C., Maslanik, J., Key, J., & Emery, W. (2002). *AVHRR Polar Pathfinder twice-daily 1.25 km EASE-Grid composites*. Technical Report Boulder. CO, USA: National Snow and Ice Data Center.
Schaaf, C. B., Gao, F., Strahler, A. H., Lucht, W., Li, X., Tsang, T., et al. (2002). First operational BRDF, albedo nadir reflectance products from MODIS. *Remote Sensing of Environment*, 135−148.
Schaepman-Strub, G., Schaepman, M. E., Painter, T. H., Dangel, S., & Martonchik, J. V. (2006). Reflectance quantities in optical remote sensing − Definitions and case studies. *Remote Sensing of Environment*, 27−42.
Schmidt, T., & König-Langlo, G. (1994). Radiation measurements at the German Antarctic Station Neumayer 1982–1992. *Rep. Polar. Res., vol. 146*, Bremerhaven, Germany: Alfred Wegener Institute for Polar and Marine Research 65 pp.
Schulz, J., Albert, P., Behr, H. -D., Caprion, D., Deneke, H., Dewitte, S., et al. (2009). Operational climate monitoring from space: The EUMETSAT satellite application facility on climate monitoring (CM-SAF). *Atmospheric Chemistry and Physics*, 1−23.
Serreze, M., Barrett, A., Stroeve, J., Kindig, D., & Holland, M. (2009). The emergence of surface-based Arctic amplification. *The Cryosphere*, 11−19.
Smith, D. M. (1996). Extraction of winter total sea–ice concentration in the Greenland and Barents Seas from SSM/I data. *International Journal of Remote Sensing*, *17*, 2625−2646.
Steffen, K. (2009). Personal communication
Stroeve, J. (2001). Assessment of Greenland albedo variability from the advanced very high resolution radiometer polar pathfinder data set. *Journal of Geophysical Research*, 33989−34006.
Stroeve, J. C., Box, J. E., Fowler, C., Haran, T., & Key, J. (2001). Intercomparison between in situ and AVHRR polar pathfinder-derived surface albedo over Greenland. *Remote Sensing of Environment*, 360−374.
Stroeve, J., Box, J. E., Gao, F., Liang, S., Nolin, A., & Schaaf, C. (2005). Accuracy assessment of the MODIS 16-day albedo product for snow: comparisons with Greenland in situ measurements. *Remote Sensing of Environment*, 46−60.
Stroeve, J. C., Box, J. E., & Haran, T. (2006). Evaluation of the MODIS (MOD10A1) daily snow product over the Greenland ice sheet. *Remote Sensing of Environment*, 155−171.
Stroeve, J., Nolin, A., & Steffen, K. (1997). Comparison of AVHRR-derived and in situ surface albedo over the Greenland ice sheet. *Remote Sensing of Environment*, 262−276.
Vihma, T., Jaagus, J., Jakobson, E., & Palo, T. (2008). Meteorological conditions in the Arctic Ocean in spring and summer 2007 as recorded on the drifting ice station tara. *Geophysical Research Letters*, L18706.
Vihma, T., Johansson, M., & Launiainen, J. (2009). Radiative and turbulent surface heat fluxes over sea ice in the western Weddell Sea in early summer. *Journal of Geophysical Research*. doi:10.1029/2008JC004995
Wang, X., & Key, J. R. (2004). Arctic surface, cloud, and radiation properties based on the AVHRR polar pathfinder dataset. part I: Spatial and temporal characteristics. *Journal of Climate*, 2558−2574.
Weeks, W., & Ackley, S. F. (1982). *The growth, structure, and properties of sea ice. volume 82-1 of CRREL Monograph*. US Army Corps of Engineers, Cold Regions Research & Engineering Laboratory.
Xiong, X., Stamnes, K., & Lubin, D. (2002). Surface albedo over the Arctic Ocean derived from AVHRR and its validation with SHEBA data. *Journal of Applied Meteorology*, 413−425.